Catalysis Today 158 (2010) 78–88

Contents lists available at ScienceDirect

Catalysis Today

journal homepage: www.elsevier.com/locate/cattod

Study of nanoporous catalysts in the selective catalytic reduction of NO_x

María José Orellana Rico [a], Ramón Moreno-Tost [a], Antonio Jiménez-López [a], Enrique Rodríguez-Castellón [a,*], Rosa Pereñíguez [b], Alfonso Caballero [b], Juan Pedro Holgado [b]

[a] Departamento de Química Inorgánica, Cristalografía y Mineralogía (Unidad Asociada al ICP-CSIC), Facultad de Ciencias, Universidad de Málaga, Campus de Teatinos, 29071 Málaga, Spain
[b] Departamento de Química Inorgánica e Instituto de Ciencia de Materiales de Sevilla, Universidad de Sevilla-CSIC, Av. Americo Vespucio s/n, 41092 Sevilla, Spain

ARTICLE INFO

Article history:
Available online 26 May 2010

Keywords:
SCR of NO
SBA-15
XANES
Operando
Factor analysis
Copper

ABSTRACT

Two SBA-15 type materials were synthesized using a low-cost route, a pure silica SBA-15 and an Al containing SBA-15 (with a Si/Al ratio of 10), where Al was added by a post-synthesis modification. The later solid was achieved without any significant loss in the textural properties of SBA-15, besides improving its properties as support of catalysts. Copper impregnated catalysts were prepared through the incipient wetness impregnation of the two supports. With both supports, the copper weight loading were 1, 3 and 6 wt%. The copper incorporation kept the support mesoporous structures, obtaining a better dispersion of the active phase in the containing aluminium support. All the catalysts showed a moderated catalytic activity in the SCR of NO with propane in presence of an excess of oxygen in the whole studied interval of temperatures and a much better performance was observed when using NH_3 instead of propane. The changes of the active phases were studied by operando XAS spectroscopy. Factor analysis of in operando XANES results with sample SiAl_6 indicate that no Cu^0 was detected, but only Cu^{1+} and Cu^{2+}. The temperature where the Cu^{1+}/Cu^{2+} ratio is maximum occurs at the reaction temperature where the observed catalytic NO conversion is also maximum.

1. Introduction

Copper catalysts have attracted much attention in the field of NO abatement during the last decades since the early works of Iwamoto et al. [1,2], where they reported the high activity of Cu-ZSM-5 catalysts in the direct decomposition of NO into N_2 and O_2 as well as in the SCR of NO with hydrocarbons [3,4]. Although, Cu-ZSM-5 catalyst displays a poor hydrothermal stability in real operation conditions, it has been used as a "model catalyst" from which has been generated a vast number of catalysts active in the decomposition of NO so as in the SCR of NO with hydrocarbons. Since then, in the scientific literature, there is a huge amount of data concerning the catalytic performance of copper catalysts in the SCR of NO with hydrocarbons, being the zeolites the main used supports. These works cover a great variety of studies including kinetics and mechanistic studies [5–9], FTIR characterization [10–15] of adsorbed species arisen either after adsorption of probe molecules to estimate the copper species present in the copper catalysts or in realistic catalytic conditions to determinate a reaction mechanism, and studies of oxidation state of copper [5,16–23] by XAS spectroscopy before and after catalytic performance. To understand the catalytic behaviour of the copper species involved in the reaction is necessary to knowledge the oxidation and coordination copper ions in the supports in this way we can understand the nature of the active centres in the working catalyst [20].

X-ray absorption spectroscopy (XAS) can be applied to investigate catalysts under real working conditions of temperature and composition of the reactive gases. For example, Liu et al. [16] investigated on the mechanism of NO selective catalytic reduction (SCR) by hydrocarbon over Cu-ZSM-5, focused on the oxidation state and coordination chemistry of the exchanged Cu as the active site during the catalytic reaction using XAS techniques. These authors demonstrated the existence of a redox mechanism which involves cyclic switching of the oxidation states between Cu^{2+} and Cu^{1+} in an oxygen-rich gas mixture under elevated temperature. A correlation between cuprous ion concentration and catalytic activity was found in NO SCR by propene, propane and methane. Caballero et al. [17] studied by means of X-ray absorption spectroscopy the chemical state of copper in Cu/ZrO_2 catalysts under different reaction conditions. The first derivative of the X-ray absorption near-edge structure (XANES) spectra of the Cu K edge was analysed by factor analysis (FA). This analysis provided an accurate mean of estimating the percentages of Cu^{2+}, Cu^+, and Cu^0 under each reaction condition. When the catalyst was treated at 773 K with mixtures consisting of hydrocarbons (propane, propene or methane) plus NO, there was a significant concentration of Cu^+ and Cu^0 species, although

* Corresponding author. Tel.: +34 952131873; fax: +34 952132000.
E-mail address: castellon@uma.es (E. Rodríguez-Castellón).

0920-5861/$ – see front matter © 2010 Elsevier B.V. All rights reserved.
doi:10.1016/j.cattod.2010.04.016

the relative concentration of Cu^{2+} generally increased. For these gas mixtures, it was also found that the relative concentration of the three different oxidation states of copper was highly dependent on the type of hydrocarbon. In general, the concentration of reduced species was related to the reactivity of the hydrocarbon ($CH_4 < C_3H_8 < C_3H_6$) and was particularly high with C_3H_6. Finally, the analysis showed that most copper remained as Cu^{2+} when the sample was heated in a hydrocarbon/NO/O_2 mixture at 773 K, although some Cu^+ can persist under these conditions.

The ordered mesoporous materials have been tested as supports of catalysts in the SCR of NO with hydrocarbons and ammonia [6,24–29]. Within the family of mesoporous materials, SBA-15 materials synthesized under acidic conditions exhibit larger pore size and thicker pore wall compared with M41S materials. The improved hydrothermal and thermal stability makes them very promising catalytic materials [30]. Moreover, the doping elements such as aluminium, titanium and zirconium can be incorporated into the silica framework to obtain materials for applications such as catalysis and ion exchange. Recently, our group has successfully incorporated aluminium into a mesoporous silica with SBA-15 structure via a post-synthetic method [31]. The introduction of Al into the structure of SBA-15 enhances its acidity which may promote the SCR reactions [32,33]. Thus, we prepared a family of copper catalysts based on aluminium grafted mesoporous SBA-15 silica to test in the SCR of NO with propane and ammonia. The catalysts have been characterized by means of several techniques and, moreover, we have characterized in situ the catalysts in modo operando by XANES in order to know the oxidation state of copper in the realistic conditions of catalytic performance.

2. Experimental

2.1. Catalysts preparation

2.1.1. Reactants

The silicon source was a sodium silicate solution ($Na_2Si_3O_7$ with 27% SiO_2 and 14% NaOH from Aldrich). Aluminium was incorporated with aluminium chloride ($AlCl_3{\cdot}6H_2O$) from Aldrich. The non-ionic surfactant was triblock poly(ethylene oxide)-b-poly(propylene oxide)-b-poly(ethylene oxide) copolymer Pluronic P123 (M_{av} = 5800, $EO_{20}PO_{70}EO_{20}$) from Aldrich. Analytical grade sodium hydroxide from Prolabo and tetramethylammonium hydroxide (TMAOH) 25 wt% solution in water from Aldrich were also used. The source of copper was $Cu(NO_3)_2{\cdot}3H_2O$ supplied by Merck.

2.1.2. Catalysts preparation

The support synthesis has been carried out according to the procedure described by Gómez-Cazalilla et al. [31]. In a typical synthesis, 5 g of Pluronic were added to 200 mL of 0.4 M H_2SO_4 solution and stirring until a clear solution was obtained. Then, 0.2 g of NaOH and 13.3 mL of sodium silicate solution were added at room temperature with magnetic stirring. The resulting gel mixture was stirred for 5 days at room temperature; the final pH was about 1. The solid product was recovered by filtration, washed several times with water and dried overnight at 333 K. Finally, the material was heated in air at a heating rate of 10 K min^{-1} to 823 K and maintained at this temperature for 6 h. The pure mesoporous silica is labelled as Si. Alumination of this pure silica Si-SBA-15 material was carried out by mixing the appropriate volume of aqueous solution 1.2 M of $AlCl_3{\cdot}6H_2O$ with 25 mL of TMAOH 5.5 wt% solution in water to obtain a Si/Al molar ratio of 10. The resulting acid solution (pH 3.5–4) was heated to 353 K until a clear solution was obtained (ca. 1 h). Then 1.5 g of the pure silica Si-SBA-15 was added at room temperature and this mixture was maintained at 353 K for 3 h. After filtration, washing with water and drying at 333 K, the products were calcined with a heating rate of 10 K min^{-1} to 823 K and maintained at this temperature for 6 h. The aluminated support was labelled as SiAl.

Catalysts with copper loading ranging between 1 and 12 wt% were prepared by means of wet incipient impregnation method. Thus, 2 g of aluminated support was put in contact with an aqueous solution of copper(II) nitrate. After impregnation, the catalysts were dried at 333 K and calcined at 623 K (2 K min^{-1}, heating rate) during 4 h. The copper catalysts were labelled as Si_*x* or SiAl_*x* where *x* is referred to copper loading and Si and SiAl are referred to the composition of the support.

2.2. Catalysts characterization

The Al and Cu contents of the support and catalysts were measured by atomic absorption spectroscopy using a Varian SPECTRAA50. Powder XRD measurements were performed on a Siemens D5000 automated diffractometer, over a 2θ range with Bragg–Brentano geometry using the Cu Kα radiation and a graphite monochromator. X-ray photoelectron spectroscopy (XPS) studies were performed with a Physical Electronics PHI 5700 spectrometer equipped with a hemispherical electron analyzer (model 80-365B) and Al an Mg Kα (1486.6 eV and 1253.6 eV, respectively) X-ray sources. Short acquisition time of 10 min was used to examine C 1s, Cu 2p XPS regions in order to avoid, as much as possible, photoreduction of Cu^{2+} species. Nevertheless, a Cu^{2+} reduction in high vacuum during the analysis cannot be excluded [34]. High-resolution spectra were recorded at 458 take-off-angle by a concentric hemispherical analyzer operating in the constant pass energy mode at 29.35 eV, using a 720 mm diameter analysis area. Charge referencing was done against adventitious carbon (C 1s at 284.8 eV). The pressure in the analysis chamber was kept lower than 5×10^{-6} Pa. PHI ACCESS ESCA-V6.0 F software package was used for data acquisition and analysis. A Shirley-type background was subtracted from the signals. Recorded spectra were always fitted using Gauss–Lorentz curves in order to determine more accurately the binding energy of the different element core levels.

N_2 adsorption–desorption isotherm at 77 K was obtained using an ASAP 2020 model of gas adsorption analyzer from Micromeritics, Inc. Prior to N_2 adsorption, the samples were evacuated at 473 K (heating rate 10 K min^{-1}) for 1 h. Pore size distribution and pore volume were calculated with the BJH method. Temperature-programmed reduction with hydrogen (H_2-TPR) of catalysts was studied between room temperature and 673 K, using an Ar/H_2 flow of 40 cm^3 min^{-1} (10 vol.% of H_2) and a heating rate of 10 K min^{-1}. The water produced in the reduction reaction was trapped by passing the gas flow through a cold finger at 193 K. Hydrogen consumption was monitored by an on-line gas chromatograph provided with a TC detector.

Copper surface area and dispersion were calculated by N_2O decomposition method [35,36]. This method is based in the formation of a monolayer of Cu_2O by oxidation of Cu^0 with a flowing of N_2O according to the reaction:

$$2Cu^0 + N_2O \rightarrow Cu_2O + N_2$$

Before analysis, the CuO phase is reduced by a H_2-TPR in a flow mixture of 10 vol.% H_2/Ar at 5 K min^{-1} up to 673 K, taking place the next reaction:

$$CuO + H_2 \rightarrow Cu + H_2O$$

Then, the catalyst is purged in He and cooled down to 333 K. The oxidation of Cu^0 to Cu^+ is carried out by the chemisorption of N_2O (5 vol.% N_2O/He) at 333 K during 1 h:

$$2Cu^0 + N_2O \rightarrow Cu_2O + N_2$$

In sequence, the catalyst was again purged in an Ar flow and cooled to room temperature. After this, s-TPR was carried out similarly to TPR, raising the temperature up to 723 K on the freshly oxidized Cu_2O surface in order to reduce Cu_2O to Cu.

2.3. Catalysis

Catalysts were tested in the SCR of NO by using a Pyrex glass tube microreactor (6.85 mm o.d.) working at atmospheric pressure in a steady-state flow mode and with a catalytic charge of 150 mg of pelletised solids, sieved to 0.3–0.4 mm, in all cases without dilution. Samples were pre-treated at 623 K in situ for 2 h under a He flow (30 cm^3 min^{-1}). The gas reaction mixture was composed of 1000 ppm NO, 1000 ppm NH_3 or propane and 2.5 vol.% O_2 (balanced with helium). In some tests, 13 vol.% H_2O, passing helium through a saturator with deionized water and 56 ppm of SO_2, was added to the feed stream. The flows were independently controlled by channel mass flowmeters (Brooks) and a total flow rate of 75 cm^3 min^{-1} was used in the feed. The space velocity (GHSV) was 1886 h^{-1}; in these conditions, both external and internal diffusional limitations were absent. The reaction was studied from 373 to 823 K. The analysis of reactants and products was monitored by using the online quadrupole mass spectrometer described above. In previous experiments, variation in the amount of catalyst with a total flow rate maintaining the space velocity constant produced no modification of conversion values. No influence of the particle diameter was found either.

2.4. XAS-In operando: SCR-NH_3 and SCR-NH_3 + H_2O

XAS spectra were recorded at the BM25 beam line (SPLINE) of the ESRF synchrotron (Grenoble, France). The spectra were acquired in transmission mode using a modified Specac infrared-transmission cell with Kapton windows that allow "operando" treatment of the sample under controlled gas mixtures and temperatures. The sample was placed in a stainless steel holder directly in contact with the gas mixture atmosphere and resistively heated. The samples were pressed as self-supported wafers in a standard 13 mm diameter, using the optimum weight to maximise the signal-to-noise ratio in the ionisation chambers. For energy calibration, a standard Cu foil was introduced after the ionisation chamber (I_1) and measured simultaneously. Typical EXAFS spectra of Cu K edge were recorded from 8905 to 9730 eV, with a variable step energy value, and a minimum 0.5 eV step across the XANES region (8970–9010 eV). For the reaction treatments, NO, NH_3 and O_2 (1000 ppm, 1000 ppm and 2.5% respectively) were diluted in He, using mass flow controllers for dosing the gases to the cell and a total flow of 115 mL min^{-1}. The effect of a flow of 10 wt% of H_2O was also studied, using a Fresenius "Orchestra" perfusor for injecting the water onto the NO/NH_3/O_2/He mixture, being all the pipes from this point up to cell heated at 353 K to avoid water condensation. The catalysts were pre-treated in He from room temperature to 773 K, and cooling down in He, after that the mixture was introduced in the cell at room temperature and then heated to the desired temperature (from RT to 773 K) using a ramp of 10 K min^{-1}. Analysis of the XANES spectra was performed using Factor Analysis on the derivatives of the original spectra, according with the procedure already described [17].

3. Results and discussion

3.1. Catalysts characterization

The small-angle powder XRD patterns of calcined Si and SiAl materials are shown in Fig. 1a. Both the samples exhibit XRD patterns with a very intense diffraction peak at $2\theta = 1.14^\circ$ and three other weak peaks at $2\theta = 1.95^\circ$, 2.23°, and 2.99° and diffraction peaks at 1.15°, 2.00°, 2.28° and 3.02° for Si and SiAl materials, respectively, which can be indexed in a system of hexagonal symmetry as (1 0 0), (1 1 0), (2 0 0) and (2 1 0) diffraction planes, respectively. The XRD diffraction peaks can be indexed to a hexagonal lattice with a d_{100} spacing close to 8.0 nm, corresponding to a unit cell parameter a_0 of 8.9 nm, based on the formula $a_0 = 2d_{100}/\sqrt{3}$. After alumination, the XRD patterns indicate that all this support retains the characteristic patterns of the hexagonal mesostructure.

Table 1
Textural parameters of supports and copper catalysts.

Catalyst	S_{BET} (m^2 g^{-1})	V_p (cm^3 g^{-1})	d_p (nm)
Si	333	0.38	3.1
Si_1	298	0.34	3.2
Si_3	261	0.29	3.1
Si_6	259	0.30	3.2
SiAl	262	0.27	2.9
SiAl_1	243	0.25	3.0
SiAl_3	229	0.24	3.0
SiAl_6	202	0.21	3.0

Table 2
Copper dispersion, metallic surface and particle size determined by means of N_2O decomposition reaction and particle size determined by means of Scherrer equation.

Catalyst	D_{Cu}[a] (%)	S_{Cu}[a] (m^2 Cu g Cu^{-1})	d_{av}[a] (nm)
Si_1	54%	363.1	1.9
Si_3	11%	77.1	8.8
Si_6	9%	61.8	10.9
SiAl_1	99%	670.9	1.0
SiAl_3	57%	383.6	1.8
SiAl_6	15%	100.0	6.8

[a] N_2O decomposition reaction.

The main textural parameters of supports and copper catalysts are compiled in Table 1. As it is shown, the incorporation of aluminium to the Si support involves a decrease of the S_{BET}, main pore size and pore volume values, according to Gómez-Cazalilla et al. [31], this fact could be indicative of the incorporation of the aluminium into the pore surface of the Si support. The aluminium could be incorporate by partial substitution of Si atoms. The value of the inorganic wall thickness of the material, calculated from the main pore diameter and XRD data, increases from 5.85 to 5.99 nm when the aluminium is incorporated into the Si solid, therefore, this change in the wall thickness could also point out the incorporation of the aluminium into the pore surface of the Si material. On the other hand, the Si and SiAl supports display a monomodal pore size distribution. After deposition of CuO on the supports, it was caused a lowering of both pore volume and specific surface of Si and SiAl as the copper loading is increased.

The XRD patterns of the Si_*x* and SiAl_*x* catalysts show, besides a very broad band at 20–30° 2θ, typical of unstructured silica groups, diffraction peaks corresponding to the presence of CuO particles (Fig. 1b). As it is shown, the catalysts based on Si support show more intense diffraction peaks than their counterparts. Moreover, the intensity of the peaks increases with the copper loading. By this technique no new crystalline oxide phases formation between CuO and aluminium species are detected. Thus, it could be concluded that the presence of Al increases the dispersion of the CuO particles over the support. A first rough estimation of the CuO particle dimensions was performed from the broadening of the peak at 35° by the Scherrer formula. The Scherrer equation has been just applied to Si_*x* since the broadening of the peak of the SiAl_*x* catalysts prevents the analysis of the particle size. CuO particle sizes between 50 and 60 nm have been obtained (Table 2).

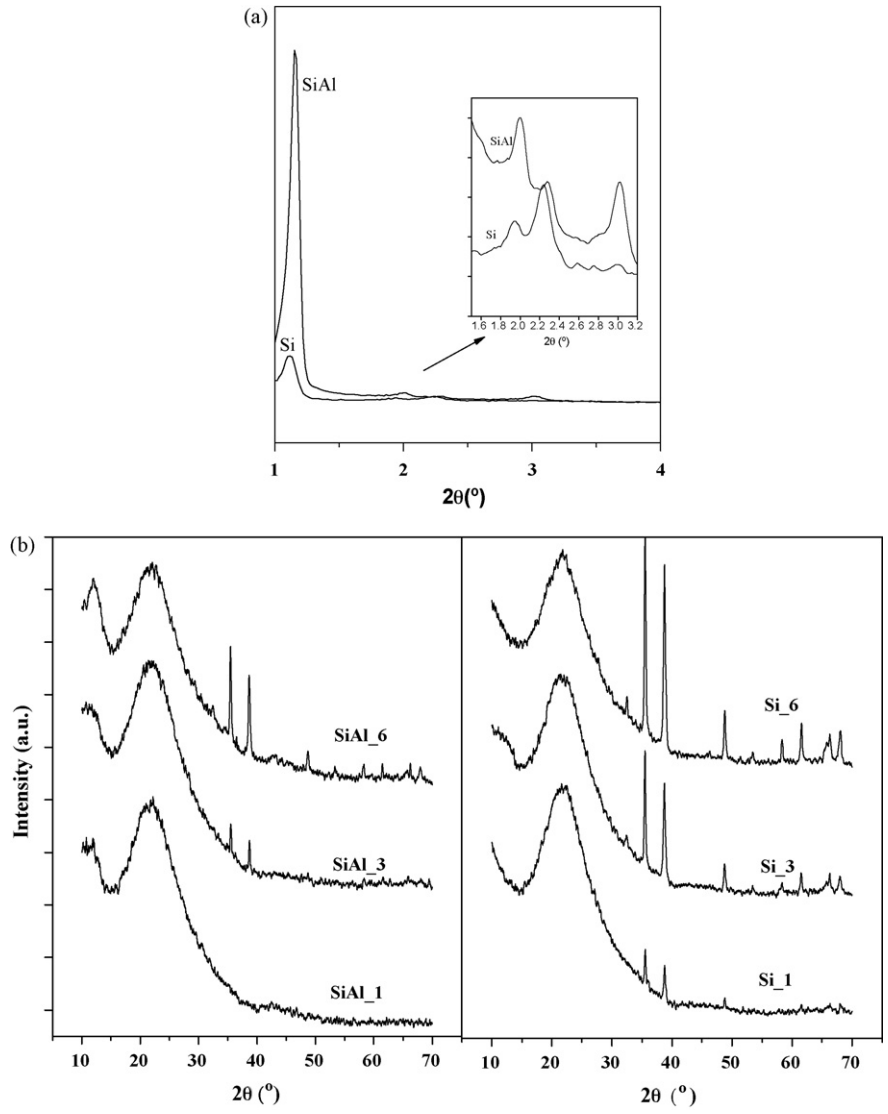

Fig. 1. Powder XRD patterns of Si and SiAl supports (a), Si_*x* and SiAl_*x* catalysts (b).

The free copper surface area and particle size of the individual copper crystallites can be measured by a large number of techniques, being the reaction of N_2O decomposition method widely accepted to determinate the particle size, copper dispersion and copper surface area. Thus, copper dispersion (D_{Cu}), defined as the ratio of Cu exposed at the surface to total Cu present, was calculated from the amount of H_2 consumed in the TPR analysis. H_2 consumption (from TPR) can also be used to calculate the copper metal surface area (S_{Cu}) and the average particle size (d_{av}) by means of the following assumptions and equations:

The area per copper surface atom in (1 0 0), (1 1 0), and (1 1 1) planes are 0.065, 0.092, and 0.056 nm^2, respectively [37] An equal abundance of these three planes give an average copper surface atom area of 0.071 nm^2, equivalent to 1.4×10^{19} copper atoms per square meter. By assuming a spherical shape of the copper metal particles, S_{Cu} and d_{av} can be expressed as, respectively,

$$S_{Cu}\,(m^2\,g_{Cu}{}^{-1}) = Mol_{H_2} \cdot SF \cdot \frac{N_A}{10^4 C_M \cdot W_{Cu}}$$

$$d_{av}\,(nm) = \frac{6000}{S_{Cu} \cdot \rho_{Cu}}$$

where Mol_{H_2}, SF, N_A, C_M, W_{Cu}, and ρ_{Cu} are moles of hydrogen experimentally consumed per unit mass of catalyst (μmol H_2 g^{-1} cat), stoichiometric factor (2), Avogadro's number (6.022×10^{23} mol^{-1}), number of surface Cu atoms per unit surface area, Cu content (wt %), and the density of copper (8.92 g cm^{-3}).

The Cu percentage dispersion, metal surface area, and average particle size are given in Table 2. It was shown that the dispersion and metal area of copper are decreased with copper loading whereas average particle size is increased with copper loading. This effect is more marked for the catalysts based on Si support. On the other hand, the SiAl_1 shows the highest Cu dispersion and S_{Cu} exposed. This might indicate the maximum number of dispersed copper sites that are available on the catalyst surface. Thus, increasing the copper loading, the dispersion and metal area are decreased, and average particle size is increased beyond this loading due to formation of CuO crystallites. This is in good agreement with XRD data in the sense of increasing the particle size with the copper loading. Therefore, the aluminium doped mesoporous silica dispersed the copper oxide in a higher extension than pure mesoporous silica. In literature, it is observed an increase of the dispersion with the copper loading up to a determinate level which depends on the support and the method of preparation of catalysts. Thus, Komandur et al. [38] reported beyond 2.7 wt% a decrease of copper disper-

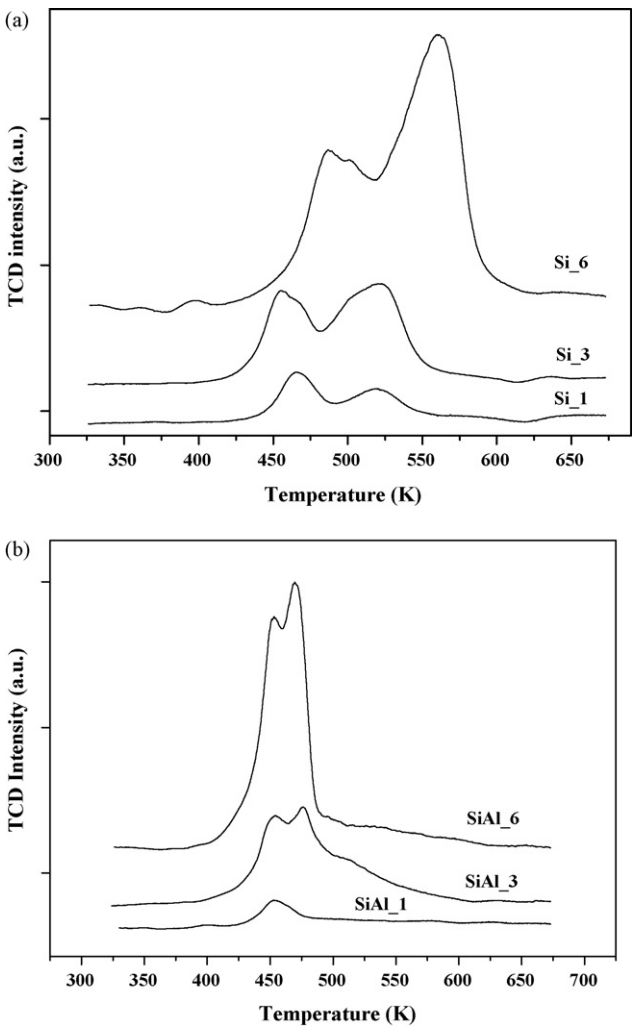

Fig. 2. H_2-TPR curves of Si_*x* (a) and SiAl_*x* (b) catalysts.

sion in the case of copper supported on ZrO_2. This copper loading which the maximum copper dispersion is reached, is increased up to 5 wt% when mixed Al_2O_3–ZrO_2 oxides are used as supports [39]. These authors reported similar results for Cu supported on mixed TiO_2–ZrO_2 oxides [40].

The reduction of Cu species was studied by H_2-TPR experiment. The reduction profile provides information on the dispersion of metal species over the support and the interaction between the metal ions and the support [41]. The TPR profiles of Si_*x* and SiAl_*x* catalysts are shown in Fig. 2a and b, respectively. The catalysts show different H_2 consumption profiles depending on either the support or Cu loading. Thus, the Si_*x* catalysts show two well resolved reduction peaks whereas SiAl_*x* catalysts, depending on the Cu loading, may show one or two reduction peaks. This suggests the presence of different copper species on the supports. The SiAl_*x* catalyst shows an unique reduction peak at 453 K and both SiAl_3 and SiAl_6 catalysts shows two reduction peaks, the first at 453 K and the second one at 476 and 469 K for SiAl_3 and SiAl_6 catalysts, respectively. The intensity of both reduction peaks is increased with the copper loading, being the peak at low temperature ascribed to highly dispersed surface CuO species and the peak at higher temperature is attributed to bulk-like CuO particles, therefore, it can be concluded the CuO is highly dispersed in the SiAl_1 catalyst, as the previous XRD data shown since this catalyst did not show any diffraction peak attributable to crystalline CuO. This behaviour of supported CuO has been already reported by several authors. Chary et al. [39] studied the copper phases present over Al_2O_3–ZrO_2 support by means of H_2-TPR. They concluded that at low copper loading (<5 wt%), the CuO are present as well-dispersed CuO species and crystalline copper oxide species at high Cu loadings (>10 wt%). These same results were reported [43] studying the dispersion of CuO over ZrO_2. Gervasini et al. [42] reported the presence of fine dispersed CuO_x particles and CuO aggregates as function of copper loading on SiO_2–Al_2O_3 support. On the other hand, the intensity of the two peaks is relatively comparable which could entail a same distribution of the two kinds of CuO particles on the SBA-SiAl support.

The Si_*x* catalysts also display two H_2 consumption peaks. These peaks are assigned to CuO_x species (peak at 453–561 K) and bulk-like CuO particles (peak at 520–560 K), respectively. The intensity of both peaks is increased and they are shifted at higher temperatures with the copper loading. Furthermore, the intensity of the reduction peak at high temperature becomes greater than the peak at lower temperature, therefore, being more abundant the bulk-like CuO particles than the highly dispersed CuO_x particles. This is in good agreement with the XRD patterns of these catalysts since they showed well-defined features of crystalline CuO. Finally, the data reported so far by XRD analysis, N_2O decomposition reaction and H_2-TPR experiments show the promoter effect of aluminium in the dispersion of CuO phases.

Finally, the surface composition and chemical state of the catalysts have been studied by means of XPS analysis. The XPS analysis confirmed the exclusive presence of Cu(II) species on all the catalyst surfaces. The bands presented clear spin–orbit split Cu $2p_{1/2}$ and Cu $2p_{3/2}$ peaks along with their shake-up satellites which are known to be characteristics of Cu(II) systems [42,44]. These satellites have been attributed to shake-up transitions by ligand → metal 3d charge transfer. This charge transfer cannot occur in Cu^+ compounds or Cu^0 because of their completely filled 3d shells [44]. Furthermore, generally, the lower binding energy (932.2–933.1 eV) and absence of shake-up peaks are characteristics of Cu^{1+} ion [28]. The binding energy values of Cu $2p_{3/2}$ peaks are listed in Table 3 for the two families of copper catalysts. Si_*x* catalysts only show a contribution of the Cu $2p_{3/2}$ peak at about 934 eV. On SiAl_1 was also detected a unique contribution of the Cu $2p_{3/2}$ peak whereas SiAl_3 and SiAl_6 catalysts show two contributions. The low energy peak (933.8 eV) can be associated with CuO while the high-energy peak (935.1) can be indicative of a charge transfer from the metal ion toward the support oxide. Kim et al. [45] ascribed this contribution to the formation of $CuAl_2O_4$ phase. These values of core level Cu 2*p* are in accordance with those reported in literature for dispersed CuO [5,44,46]. Another spectroscopy feature characteristic of the presence of Cu^{2+} is the value of the intensity ratio of the satellite peak to the corresponding photoelectronic peak (I_{sat}/I_{pp}). This value is close to 0.5 for CuO [44,47]. It has been reported that this intensity ratio is sensitive to the coordination environment, the higher the intensity the lower the coordination number of Cu^{2+} cations [47]. In the catalysts studied, it was found to be about 0.5 only for Cu6_Si sample (see Table 3). This sample was which displayed a better crystallinity as XRD pattern shown. Conversely, the I_{sat}/I_{pp} ratio was lower for all the other catalysts mainly the SiAl_*x* catalysts. Low I_{sat}/I_{pp} values suggest the presence of CuO in a highly dispersed amorphous state. It is known that nanosized particles have properties different from the bulk oxides, and this mixed oxidation state could be the result of the defective structure of the small clusters [40].

Depending on the chemical composition of the support, we might distinguish different sites on the surface of the pure silica or silica-alumina support, respectively. Thus, strong acidic groups (–Si–OH–Al–) or weakly acidic ones (–Si–OH) together with Lewis sites related with defective aluminium sites could be present and anchored the copper species. In this way, depending on the Cu load-

Table 3
XPS data of Si_*x* and SiAl_*x* catalysts.

Catalyst	BE Cu $2p_{3/2}$	BE Cu shake up	I_{sat}/I_{pp}	Cu/Si	Cu/Al
Si_1	933.8	943.3	0.336	0.010	–
Si_3	934.0	942.9	0.351	0.018	–
Si_6	933.9	941.7	0.507	0.049	–
SiAl_1	933.4	943.7	0.141	0.012	0.148
SiAl_3	932.8 (60%) 935.2 (40%)	943.7	0.311	0.040	0.255
SiAl_6	933.0 (59%) 935.1 (41%)	943.7	0.219	0.040	0.261

ing, different Cu-support interactions occurred leading to Cu-phase dispersed in a different way. The surface Cu/Si and Cu/Al ratios are compiled in Table 3 for the two families of catalysts. For the Si_*x* catalysts, it is observed an increase of Cu/Si ratio with the increase of copper loading. The fact that the amount of exposed copper increased up to 6 wt% of loading without a decrease of this ratio may indicate that the Si support could accept a higher copper loading and uniformly disperse it on the mesoporous silica surface. On the other hand, this behaviour is not found with the SiAl_*x* catalysts since such Cu/Si ratio reaches its maximum for SiAl_3 catalyst and was not increased further. Moreover, when the copper loading is increased up to 3 wt%, it is noticeable the increase of Cu/Si ratio with the copper loading for SiAl_3 compared to Si_3 catalyst (see Table 3). This is in good agreement with the XRD patterns since Si_3 catalyst already showed more intense reflection peaks corresponding to CuO diffraction planes than SiAl_3 catalyst, pointing out a poor dispersion of copper species and the formation of bigger CuO crystals. On the other hand, when copper loading is increased up to 6 wt%, it has not been measured an increase of the Cu/Si ratio. This could be due to a fraction of dispersed copper species are probably located inside of the pore network and they are not detectable by XPS. Although, the formation of larger CuO crystallites could not be ruled out since the XRD analysis also confirm detection of bulk CuO in the sample with 6 wt%. A low dispersion of copper oxide is also noticed at higher Cu loadings by the N_2O decomposition method described above. Thus, the present XPS results are in good agreement with the dispersion of copper determined by N_2O decomposition method and XRD results. Therefore, it is again demonstrated the beneficial effect of the presence of aluminium to disperse the copper species due to the essential role of acid sites on formation of CuO-active sites.

After catalytic tests, the catalysts do not show any change in the B.E. of the copper as well as Cu/Si atomic ratio indicating these results that the catalysts are very stable under the catalytic conditions.

3.2. Catalytic activity

3.2.1. Selective catalytic reduction of NO with propane

The copper catalysts have been tested in the SCR of NO with propane and ammonia as reducing agents in excess of oxygen. It is well known that for a given feed (oxygen, hydrocarbon and NO), the NO conversion depends on several experimental parameters. Thus, for instance, the temperature at the maximum activity is a function of the type of hydrocarbon, the active cation and the support [48]. On the other hand, the presence of oxygen is essential to NO reduction. Therefore, there are two reaction pathways competing for the propane oxidation which might be considered as:

$$C_3H_8 + 2NO + 4O_2 \rightarrow N_2 + 3CO_2 + 4H_2O \quad (1)$$

$$C_3H_8 + 5O_2 \rightarrow 3CO_2 + 4H_2O \quad (2)$$

Under our experimental conditions, the detected reaction products were N_2, CO_2 and NO_2 traces. Neither nitrous oxide nor CO formation was observed in the studied temperature range (623–823 K). Thus, the selectivity towards N_2 and CO_2 was of 100%

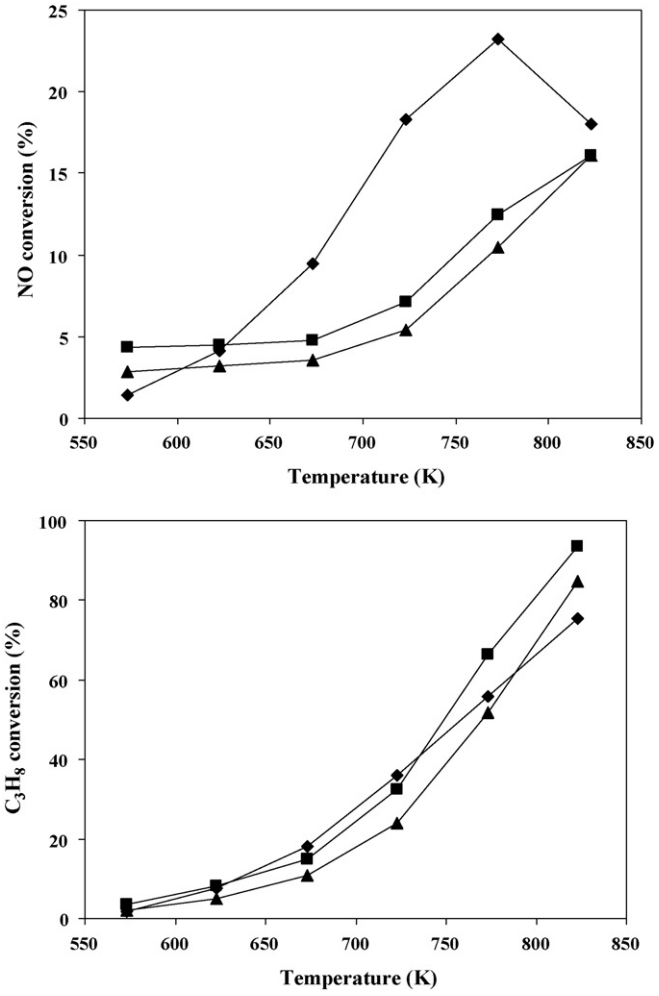

Fig. 3. NO and C_3H_8 conversion as a function of the reaction temperature for Si_*x* catalysts. Si_1 (♦), Si_3 (■) and Si_6 (▲) Experimental conditions: NO (1000 ppm), C_3H_8 (1000 ppm), O_2 (2.5 vol.%); total flow 75 ml min^{-1}.

in the whole range of temperature. Fig. 3 displays the NO conversion and C_3H_8 as function of temperature in the range of 573–823 K for the Si_*x*.

The maximum NO conversion to N_2 corresponding to Si_*x* was reached for the Si_1 catalyst at 773 K and at higher temperatures, NO conversion is depleted, leading a typical volcano-shape curve. The Si_3 and Si_6 catalysts show lower NO conversion and increase with the temperature along the temperature tested. On the other hand the conversion of propane increases with the temperature since the C_3H_8 oxidation by O_2 (reaction (2)) is prevailed over reaction (1). In fact, the SCR reaction could be explained by a reaction in which two oxidants compete for a limited available amount of reductant. In any case, it was not reached the 100% propane conversion for the all Si*x* catalysts, even at the higher temperatures tested. It is noteworthy to point out that Si_1 catalyst, among the Si*x* cat-

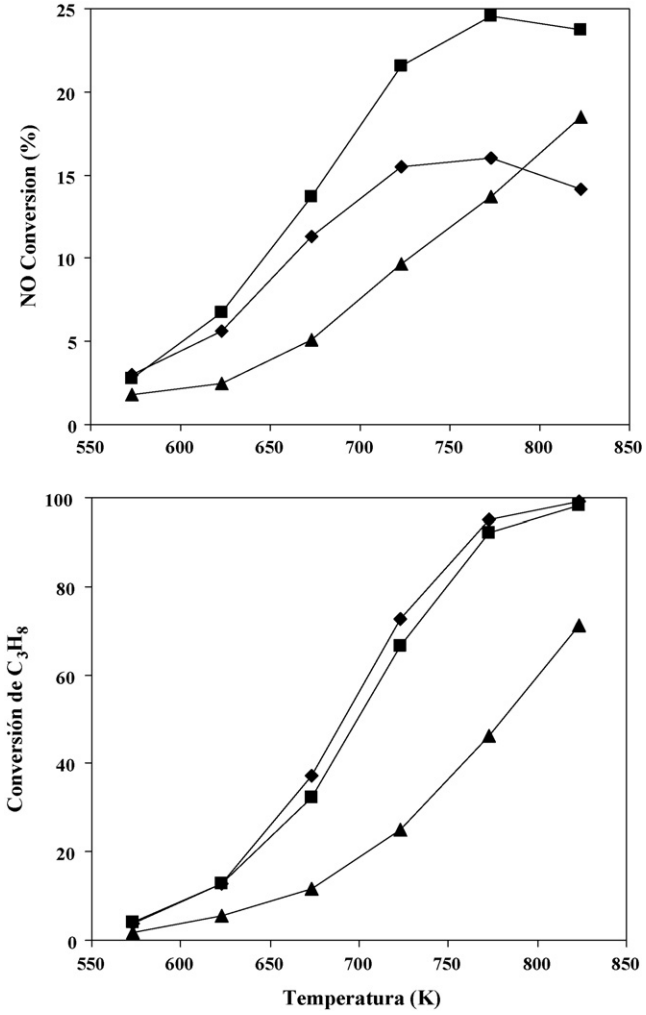

Fig. 4. NO and C_3H_8 conversion as a function of the reaction temperature for Si_*x* catalysts. SiAl_1 (▲), Si_3 (■) and SiAl_6 (♦). Experimental conditions: NO (1000 ppm), C_3H_8 (1000 ppm), O_2 (2.5 vol.%); total flow 75 ml min^{-1}.

alysts, showed the highest copper dispersion and the highest NO conversion. These results suggest that the reactivity for NO reduction by C_3H_8 is strongly depend on the copper species produced upon calcination of catalysts. It is known that bulk-like CuO particles possesses higher reactivity for C_3H_8 combustion reaction than CuO clusters or CuO_x does [42] and less reactivity for NO reduction for SCR of NO with hydrocarbons [15]. This fact was also found to copper-MFI catalysts [49] since non-isolated copper ions (copper oxides) were more active for the C_3H_8–O_2 than for the C_3H_8–NO reaction which occurred on isolated ions.

Conversely, the maximum NO conversion (~25%) corresponding to SiAl_*x* catalysts was reached for the SiAl_3 catalyst at 773 K (Fig. 4). Whereas SiAl_1 catalyst shows a linear trend of increase NO conversion with the temperature in the whole range of temperature tested, the SiAl_3 and SiAl_6 catalysts displays a typical volcano-curve of NO conversion. The copper loading increase from 3 to 6 wt% does not have a positive effect into the NO conversion, in fact, at lower temperatures (lower than 773 K) the SiAl_6 catalyst shows a better catalytic activity than SiAl_1 catalyst but at higher temperatures the catalytic behaviour of SiAl_1 surpass the SiAl_6 catalyst. This fact could be related with the formation of bigger CuO aggregates observed by XPS and the data obtained by the N_2O decomposition method. In relation to the propane conversion, SiAl_1 catalyst did not reach the complete oxidation of propane to CO_2 whereas SiAl_3 and SiAl_6 catalysts almost reach the complete

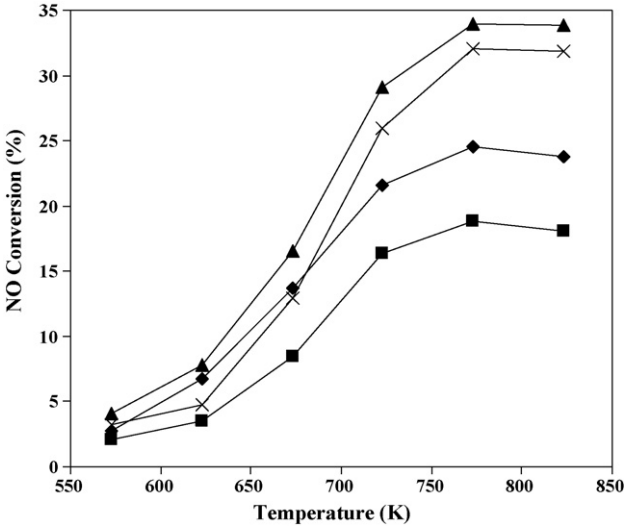

Fig. 5. NO conversion as a function of the reaction temperature for SiAl_3 catalyst catalyst as function of feed composition: standard (♦), 10 vol.% H_2O (■), 56 ppm SO_2 (▲) and H_2O with SO_2 (×). The rest of experimental conditions were the same mentioned in Fig. 3.

oxidation of propane at 823 K. Thus, the CuO_x species dispersed onto the SiAl_3 catalysts which are related to the particle size, measured by means of N_2O decomposition method and the superficial copper determined by XPS, seems to be adequate to reach the highest catalytic activity amongst the tested catalysts. It is noticeable to highlight that the properties of Si_1 and SiAl_3 catalysts are quite similar if the results of N_2O decomposition method are bearing in mind. This suggests that one of the most important properties of the copper catalysts to be active in the SCR of NO with propane is the dispersion of copper species on the surface of support. However, the role of support is not limited to exert influence in the active phase dispersion but it also exerts a basic role in the superficial characteristics of the catalysts. On contrary, Si_1 and SiAl_3 catalysts should show the same catalytic performance. As the XPS data shown, the core Cu 2p signal of Si_1 catalyst only showed a contribution ascribed to Cu^{2+} in CuO, whereas SiAl_3 catalyst showed two contributions, one of them ascribed to CuO and the other one due to the charge transfer from metal to oxidic support. Thus, CuO species with different local coordination could be present on the surface of the catalyst base on XPS data, influencing in the catalytic behaviour.

On the other hand, SiAl_3 catalyst has been tested in presence of water and SO_2 in the feed. These results are plotted in Fig. 5, showing a lowering of NO conversion if water is co-fed. This drop in NO conversion has been already reported [50,51]. The effect of water in the catalytic conversion is attributed to the adsorption of water on the active sites, being this adsorption reversible. On contrary, the NO conversion is increased when SO_2 is fed, this effect could be related to the reductor character of SO_2 which could contribute to the reduction of Cu^{2+} to Cu^{+} acting to the suitable Cu^{2+}/Cu^{+} ratio (*vide infra*).

It has been studied the effect of various experimental parameters on the catalytic activity of SiAl_6 at 723 K. Thus, it has been tested different reactant compositions varying the composition of one of the components of the feed (O_2, NO or C_3H_8) maintaining the rest constant.

The dependence of NO conversion on the oxygen content was studied using a mixture containing from 0 to 3.8 vol.% O_2 and [NO] = [C_3H_8] = 1000 ppm. The NO conversion increases up to 2.5 vol.% and then decreased (Fig. 6a). Therefore, the presence of oxygen promotes the SCR of NO by propane in the studied temper-

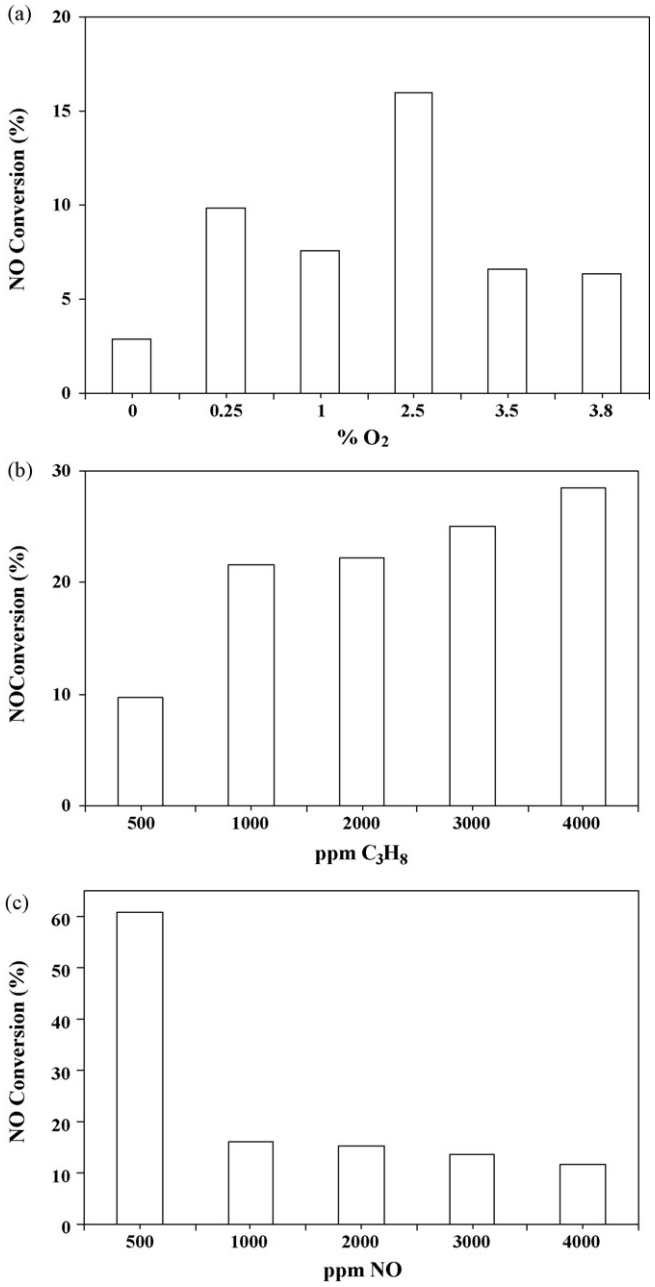

Fig. 6. Variation of NO conversion for SiAl_6 catalyst as function of: (a) oxygen concentration, (b) propane concentration and (c) NO concentration. The rest of experimental conditions were the same mentioned in Fig. 3.

ature range, but the reaction is zero order in oxygen. Interestingly, this catalyst does not display null conversion of NO in absence of oxygen. Pietrogiacomi et al. reported similar results for CuO_x/ZrO_2 catalysts [52], although those catalysts were assayed with propene instead propane. The enhanced rate by addition of excess oxygen has been related with several important factors of this reaction such as the oxidation of carbonaceous deposits, the recuperation of the Cu^{2+} oxidation state, the oxidation of NO to NO_2 and the formation of partially oxygenated hydrocarbons [53].

The dependence of NO conversion with the propane and NO content is plotted in Fig. 6b and c. Thus, the NO conversion at 723 K (Fig. 6b) is dependent on the partial pressure of propane, increasing with the propane concentration in the feed up to a value close to 30% for a concentration of 4000 ppm of propane. These results mean that for achieving a high degree of reduction of NO a slight

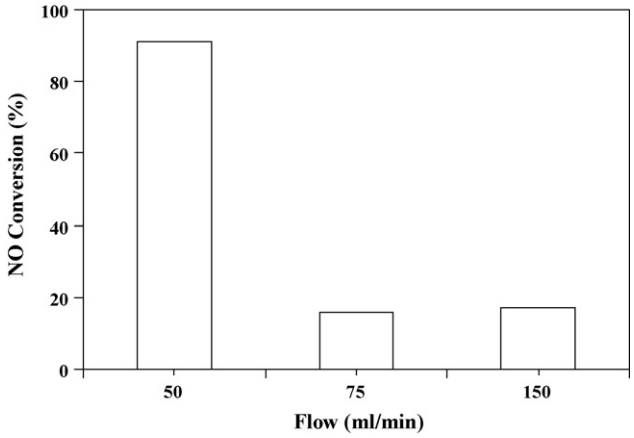

Fig. 7. Influence of GHSV in the NO conversion for SiAl_6 catalyst.

excess of propane is necessary. The evolution of NO conversion as a function of the NO composition in the feed at 723 K (Fig. 6c) shows a strongly decay in the NO conversion when the NO concentration is doubled and then it is practically maintaining up to 4000 ppm of NO. On the other hand, the evolution of the NO conversion as a function of the space velocity (GHSV values ranging between 940 and 3770 h^{-1}) reveals that the NO conversion is strongly affected by this parameter, because a sharp decrease is observed when the total flow is multiplied by two and then is maintained (Fig. 7).

Finally, the catalytic stability was studied with the SiAl_3 catalyst at 773 K during 24 h and any relevant deactivation was observed.

3.2.2. Selective catalytic reduction of NO with ammonia

Now the SCR of NO of the best catalyst (SiAl_6) is studied using NH_3 instead propane. As expected the observed conversion of NO is much higher when using NH_3 instead propane (see Fig. 8). The thermal pre-treatment also affects to the catalytic performance. When the pretreatment was performed at 723 K, the catalyst achieves a conversion of NO near to 100% at 575 K, a much lower reaction temperature than that observed with propane. However, if the sample is pre-treated at 623 K, the observed NO conversion is lower at 575 K (55%) and a maximum conversion of about 65% is observed at 625 K. In order to know "in situ" the modifications that undergoes the

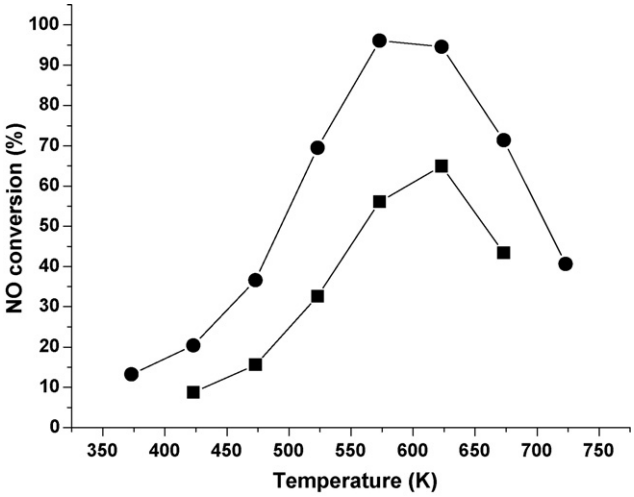

Fig. 8. NO conversion as a function of the reaction temperature for SiAl_6 petreated at 623 K (■) and 723 K (●). Experimental conditions: NO (1000 ppm), NH_3 (1000 ppm), O_2 (2.5 vol.%); total flow 75 ml min^{-1}.

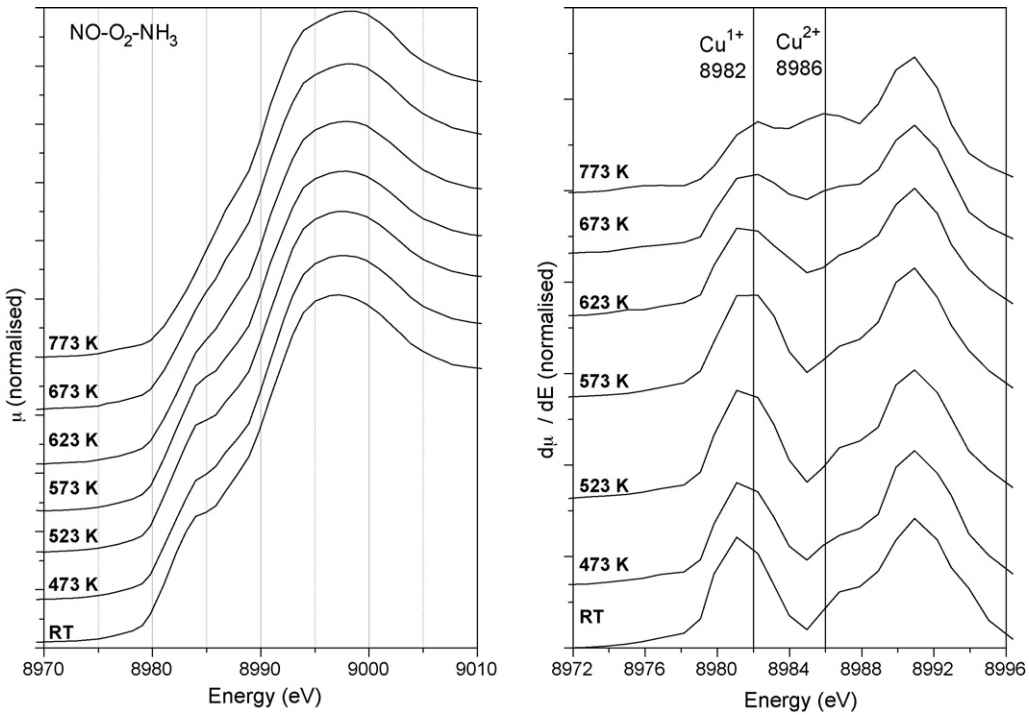

Fig. 9. Cu K edge XANES spectra of the SiAl_6 catalyst recorded "in operando" during the treatment in $NO/O_2/NH_3$ (left), and first derivative curves of these XANES spectra (right).

active phase during the catalytic reaction, XAS experiments have been designed with the sample SiAl_6 that showed the best catalytic performance,

3.3. *In operando Cu K edge XANES spectra*

The catalytic activity was not measured during XAS experiments, and although the composition of the feed was the same used in the previous catalytic test, the space velocity was slightly different in addition to the reactor geometry, and some differences in the catalytic performance are expected, but the objective of these experiments is to know the evolution of the chemical state of copper species in a more or less similar catalytic system. Fig. 9-left shows the Cu K edge XANES spectra of the SiAl_6 catalyst recorded "operando" during the treatment in $NO/O_2/NH_3$ at different reaction temperatures. In this figure, the changes in the shape

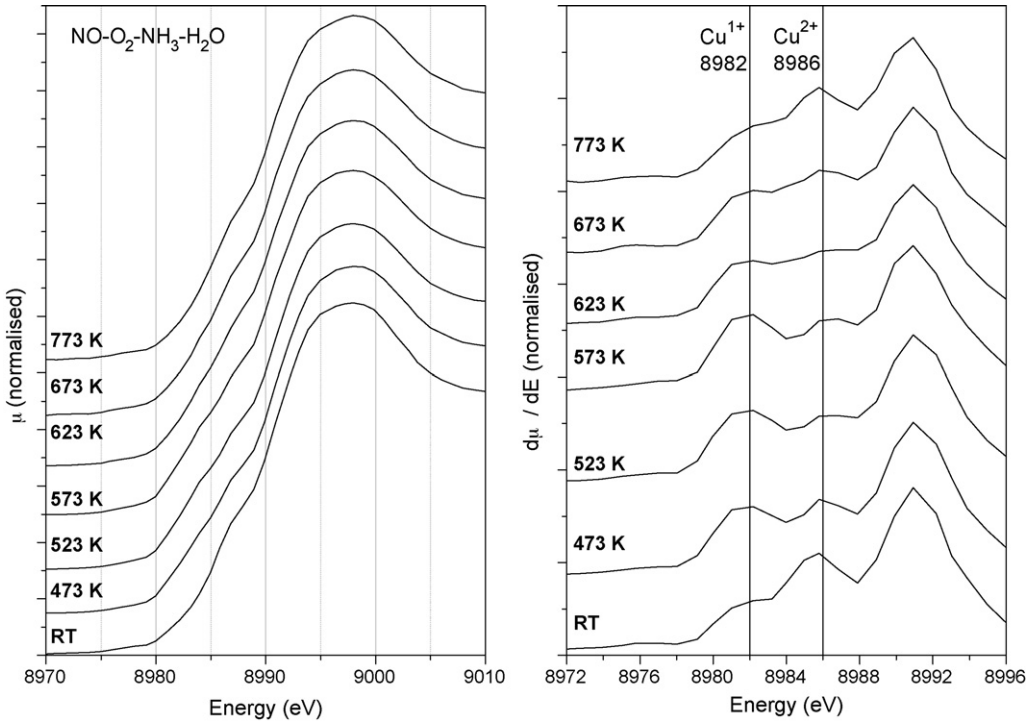

Fig. 10. Cu K edge XANES spectra of the SiAl_6 catalyst recorded "in operando" during the treatment in $NO/O_2/NH_3/H_2O$ (left), and first derivative curves of these XANES spectra (right).

of the curves registered at different reaction temperatures can be clearly observed. The most appreciable feature is the decrease of the pre-peak at around 8984 eV. Anyway, as discussed previously by some of us [17], the first derivative curves of these XANES spectra (Fig. 9-right) is more sensitive than integral curves, and the changes produced in the chemical state of the copper phase are more easily detected. The position of the principal peaks obtained for references of Cu^{1+} and Cu^{2+} are indicated also in Fig. 9. Obviously, an increase in the intensity of peaks at these energies for the catalysts subjected to different treatments is a clear indication of the formation of these species. Thus, the Cu^{1+} is the predominant species in the sample at the beginning of reaction (RT) and the intensity of this peak remains predominant until 573 K. From 573 to 773 K, the relative proportion between the intensities of Cu^{1+} and Cu^{2+} varies, getting the Cu^{2+} species more importance. At the end of the SCR-NH_3, the catalyst presents a first derivative for the spectrum that reveals a mixture of the species Cu^{1+} and Cu^{2+} in a similar proportion, due to the comparable intensity of the pointed out peaks. The XANES spectrum and its corresponding first derivative curve of the sample at room temperature, after the pre-treatment in He at 773 K, is similar to that observed in Fig. 9 at room temperature using a mixture of NO, O_2, and NH_3

Fig. 10 (left and right) shows similar qualitative assessments as Fig. 9, for the reaction $NO/O_2/NH_3 + H_2O$ at temperatures: from 473 to 773 K. The changes produces in the XANES spectra integral curves seem to be, in this case, smoother than the previous reaction, being more difficult to distinguish the chemical state of the copper in the different treatments. However, from the derivative curves of these spectra is possible to follow more clearly the presence of Cu^{1+} and Cu^{2+} species. In this case at the beginning of the reaction (room temperature) the peak corresponding to the Cu^{2+} has a higher intensity, showing clearly the more oxidative character of the reacting mixture, due to the presence of water. Increasing the temperature, the curves reveal an enhancement in the Cu^{1+} intensity and a parallel decrease in the height of the Cu^{2+} peak from room temperature to 573 K. At this point the proportion of Cu^{1+} starts to be lower again and the intensity of the peak associate to the Cu^{2+} increases with successive treatments.

3.3.1. *Factor analysis of first derivative spectra*

Although a visual inspection of the derivative curves of XANES spectra gives us an estimation of the Cu^+/Cu^{2+}, a quantitative evaluation of the relative concentration of each oxidation state of copper is possible by using the Factor Analysis technique [17]. In our case, we should firstly remark that no Cu^0 was detected, but only Cu^{1+} and Cu^{2+}, being their relative intensities plotted in Fig. 11 (left and right) for the derivative spectra in Figs. 9 and 10, respectively, including the result obtained for the pre-treatment with helium (773 K), where copper is basically as Cu^{1+}. As can be observed, for the SCR-NH_3 (Fig. 11) the proportion of Cu^{1+} remains stable nearby 0.7, from room temperature to 573 K, After this temperature, a monotonous decrease in the presence of Cu^{1+} is registered, reaching a minimum value ca. 0.4 at the highest temperature (773 K). By other way for the reaction with H_2O (Fig. 11) the percentage of Cu^{1+} at room temperature is approximately 30% and begins to rise when the temperature comes higher, getting its maximum value (ca. 50%) at 573 K. Once this temperature is overtaken, the copper phase gets more oxidized, increasing the proportion of Cu^{2+} until the end of the reaction (773 K).

In both reactions, the temperature where the percentage of Cu^{1+} is maximum, is at ca. 573 K, is the temperature where the observed catalytic NO conversion is also maximum (see Fig. 8). Depending on the gas mixture, the proportion of Cu^{1+} has a different behaviour with the temperature, being all the cases, lower for the reaction with water, reflecting the more oxidising character of the water. It is worthy to note that, as expected, when water is present, the observed catalytic conversion is also lower (not shown in this work), what indicates a clear relation between the Cu^+ and catalytic activity. It is also important to note that the stability of such Cu^+ species, has been previously correlated, with the range of stability of NO_3^- species in Cu/ZrO_2 de-NO_x catalysts [54].

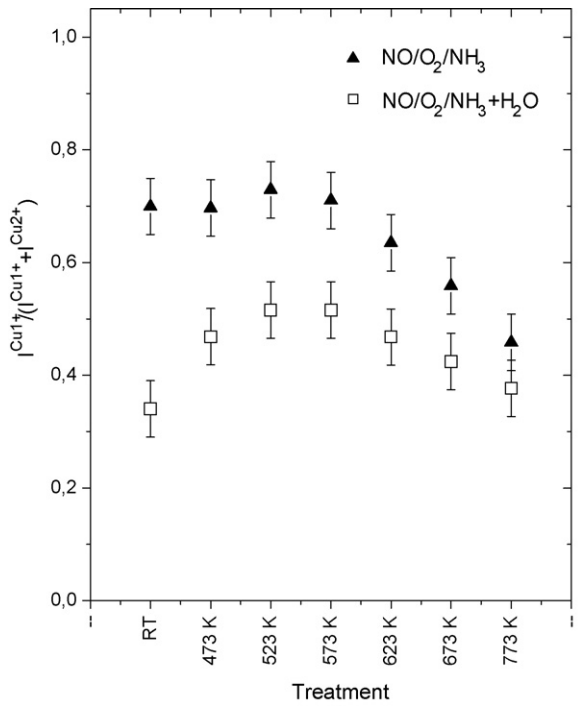

Fig. 11. Factor analysis of the first derivative spectra of Figs. 9 and 10.

4. Conclusions

Copper (1, 3 and 6 wt%) supported catalysts based on pure SBA-15 and Al containing SBA-15 were prepared and tested in the SCR of NO using propane or NH_3 as reducing agent. In both supports, the impregnated materials showed copper to be present as CuO clusters, which size increases with the increase of the copper loading. XPS analysis revealed that, in the SiAl_3 and SiAl_6 catalysts, the copper also formed a spinel-like structure $CuAl_2O_4$. All the catalysts showed a moderated catalytic activity in the SCR of NO with propane in presence of an excess of oxygen in the whole studied interval of temperatures. The influence of the total flow the propane, NO and oxygen concentration were studied. Also the SO_2 and H_2O influence on the SCR-NO was studied. The SO_2 presence produced an increase in the NO conversion, this effect could be related to the reductor character of SO_2 which could contribute to the reduction of Cu^{2+} to Cu^+ acting to the suitable $Cu^{1+}/Cu2^+$ ratio. The observed catalytic performance is much better when NH_3 is used, attaining a NO conversion of about 100% at lower reaction temperature with the catalyst SiAl_6. Factor analysis of operando XANES results with sample SiAl_6 indicate that no Cu^0 was detected, but only Cu^{1+} and Cu^{2+}. The temperature where the percentage of Cu^{1+}/Cu^{2+} is maximum, is at ca. 573 K, temperature where the observed catalytic NO conversion is also maximum.

Acknowledgements

Thanks to the Spline ESRF for beamtime access, Ministerio de Ciencia e Innovación project NAN2004-09267-C03-01 with the funding of FEDER and Project of Excellence Junta de Andalucia FQM-1661, R.M.T. would like to thanks the Ministry of Science

and Innovation (Spain) for the financial support under the Program Ramón y Cajal (RYC-2008-03387).

References

[1] M. Iwamoto, H. Furukawa, Y. Mine, F. Uemura, S. Mikuriya, S. Kagawa, J. Chem. Soc.: Chem. Commun. (1986) 1272.
[2] M. Iwamoto, H. Yahiro, K. Tanda, N. Mizuno, Y. Mine, S. Kagawa, J. Phys. Chem. 95 (1991) 3727.
[3] S. Sato, Y. Yu-u, H. Yahiro, N. Mizuno, M. Iwamoto, Appl. Catal. 70 (1991) Ll10.
[4] M. Iwamoto, H. Yahiro, S. Shundo, Y. Yu-u, N. Mizuno, Appl. Catal. 69 (1991) L15.
[5] A. Gervasini, M. Manzoli, G. Martra, A. Ponti, N. Ravasio, L. Sordelli, F. Zaccheria, J. Phys. Chem. B 110 (2006) 7851.
[6] C.C. Liu, H. Teng, Appl. Catal. B 58 (2005) 69.
[7] G. Centi, S. Perathoner, L. Dall'Olio, Appl. Catal. B 7 (1996) 359.
[8] Z. Schay, V. Samuel James, G. Pál-Borbély, A. Beck, A.V. Ramaswamy, L. Guczi, J. Mol. Catal. A 162 (2000) 191.
[9] E.V. Rebrov, A.V. Simakov, N.N. Sazonova, E.S. Stoyanov, Catal. Lett. 64 (2000) 129.
[10] T. Cheung, S.K. Bhargava, M. Hobday, K. Foger, J. Catal. 158 (1996) 301.
[11] G.D. Lei, B.J. Adelman, J. Sàrkàny, W.M.H. Sachtler, Appl. Catal. 5 (1995) 245.
[12] F. Poignant, J.L. Freysz, M. Daturi, J. Saussey, Catal. Today 70 (2001) 197.
[13] E.V. Rebrov, A.V. Simakov, N.N. Sazonova, E.S. Stoyanov, Catal. Lett. 58 (1999) 107.
[14] Z. Chajar, V. Le Chanu, M. Primet, H. Praliaud, Catal. Lett. 52 (1998) 97.
[15] O.V. Metelkina, V.V. Lunin, V.A. Sadykov, G.M. Alikina, R.V. Bunina, E.A. Paukshtis, V.B. Fenelonov, A.Yu. Derevyankin, V.I. Zaikovskii, U. Schubert, J.R.H. Ross, Catal. Lett. 78 (2002) 111.
[16] D.-J. Liu, H.J. Robota, J. Phys. Chem. B 103 (1999) 2755.
[17] A. Caballero, J.J. Morales, A.M. Cordón, J.P. Holgado, J.P. Espinós, A.R. González-Elipe, J. Catal. 235 (2005) 295.
[18] G. Turnes Palomino, S. Bordiga, A. Zecchina, G.L. Marra, C. Lamberte, J. Phys. Chem. B 104 (2000) 8641.
[19] G. Silversmit, H. Poelman, V. Balcaen, P.M. Heynderickx, M. Olea, S. Nikitenko, W. Bras, P.F. Smet, D. Poelman, R. De Gryse, M.-F. Reniers, G.B. Marin, J. Phys. Chem. Sol. 70 (2009) 1274.
[20] F.X. LlabrésiXamena, P. Fisicaro, G. Berlier, A. Zecchina, G. Turnes Palomino, C. Prestipino, S. Bordiga, E. Giamello, C. Lamberte, J. Phys. Chem. B 107 (2003) 7036.
[21] J.N. Nian, S.A. Chen, C.C. Tsai, H. Teng, J. Phys. Chem. B 110 (2006) 25817.
[22] K. Mathisen, D.G. Nicholson, A.N. Fitch, M. Stockenhuber, J. Mater. Chem. 15 (2005) 204.
[23] C. Lamberti, G. Spoto, D. Scarano, C. Pazè, M. Salvalaggio, S. Bordiga, A. Zecchina, G. Tumes Palomino, F. D'Acapito, Chem. Phys. Lett. 269 (1997) 500.
[24] Y. Wan, J. Ma, Z. Wang, W. Zhou, S. Kaliaguine, J. Catal. 227 (2004) 242.
[25] M. Boutros, J.-M. Trichard, P. Da Costa, Appl. Catal. 91 (2009) 640.
[26] R. Moreno-Tost, J. Santamaría-González, P. Maireles-Torres, E. Rodríguez-Castellón, A. Jiménez-López, Appl. Catal. 38 (2002) 51.
[27] R. Moreno-Tost, J. Santamaría-González, P. Maireles-Torres, E. Rodríguez-Castellón, A. Jiménez-López, Catal. Lett. 82 (2002) 205.
[28] R. Moreno-Tost, E. Rodríguez Castellón, A. Jiménez-López, J. Mol. Catal. A 248 (2006) 126.
[29] R. Moreno-Tost, J. Santamaría-González, E. Rodríguez-Castellón, A. Jiménez-López, Appl. Catal. B 52 (2004) 241.
[30] D. Zhao, J. Feng, Q. Huo, N. Melosh, G.H. Fredrickson, B.F. Chmelka, G.D. Stucky, Science 279 (1998) 548.
[31] M. Gómez-Cazalilla, J.M. Mérida-Robles, A. Gurbani, E. Rodríguez-Castellón, A. Jiménez-López, J. Solid State Chem. 180 (2007) 1130.
[32] X. Linag, J. Li, Q. Lin, K. Sun, Catal. Commun. 8 (2007) 1901.
[33] M. Brandhorst, J. Zajac, D.J. Jones, J. Rosière, M. Womes, A. Jimenez-López, E. Rodríguez-Castellón, Appl. Catal. B 55 (2005) 267.
[34] S. Poulston, P.M. Parlett, P. Stone, M. Bowker, Surf. Interface Anal. 24 (1996) 811.
[35] G.C. Bond, S.N. Namijo, J. Catal. 118 (1989) 507.
[36] C.J.G. van der Grift, A.E.H. Wielers, B.E.J. Joghi, J. van Beijnum, M. de Boer, M. de Boer, M. Versluijs-Helder, J.W. Sot. Geus, J. Catal. 131 (1991) 178.
[37] J.W. Evans, M.S. Wainwright, A.J. Bridgewater, D.J. Young, Appl. Catal. 7 (1983) 75.
[38] K.V.R. Chary, G. Vidya Sagar, C.S. Srikanth, V. Venkat Rao, J. Phys. Chem. B 111 (2007) 543.
[39] G. Vidya Sagar, P. Venkat Ramana Rao, C.S. Srikanth, K.V.R. Chary, J. Phys. Chem. B 110 (2006) 13881.
[40] K.V.R. Chary, G. Vidya Sagar, D. Naresh, K. Kalyana Seela, B. Sridhar, J. Phys. Chem. B 109 (2005) 9437.
[41] G. Delahay, B. Coq, L. Broussous, Appl. Catal. B 12 (1997) 49.
[42] S. Bennici, A. Gervasini, N. Ravasio, F. Zaccheria, J. Phys. Chem. B 107 (2003) 5168.
[43] K.V.R. Chary, K. Kalyana Seela, D. Naresh, P. Ramakanth, Catal. Commun. 9 (2008) 75.
[44] T.H. Fleisch, G.J. Mains, Appl. Surf. Sci. 10 (1982) 51.
[45] T.-W. Kim, M.-W. Song, H.-L. Koh, K.-L. Kim, Appl. Catal. A 210 (2001) 35.
[46] S. Bennici, P. Carniti, A. Gervasini, Catal. Lett. 98 (2004) 187.
[47] Chen S Y., Dong S L., Y.S. Lin, B. Xu, W. Ii, Stud. Surf. Sci. Catal. 101 (1996) 1293.
[48] M. Iwamoto, H. Hamada, Catal. Today 10 (1991) 57.
[49] Z. Chajar, M. Primet, H. Praliaud, J. Catal. 180 (1998) 279.
[50] R. Moreno-Tost, J. Santamaría-González, E. Rodríguez-Castellón, A. Jiménez-López, M.A. Autié, E. González, M. Carreras-Glacial, C. de las Pozas, Appl. Catal. B 50 (2004) 279.
[51] Y. Wan, J. Ma, Z. Wang, W. Zhou, S. Kaliaguine, J. Catal. 227 (2004).
[52] D. Pietrogiacomi, D. Sannino, S. Tuti, P. Ciambelli, V. Indovina, M. Occhiuzzi, F. Pepe, Appl. Catal. B 21 (1999) 141.
[53] J.O. Petunchi, W.K. Hall, Appl. Catal. B 2 (1993) L17.
[54] J. Morales, A. Caballero, J.P. Holgado, J.P. Espinos, A.R. Gonzalez-Elipe, J. Phys. Chem. B 106 (2002) 10185.